

some decohering influences here. All quasi-particle states in the superconductor have to remain unoccupied. In equilibrium, the number is far below 1 at temperatures below 30 mK. Extreme care must be taken to shield the sample from photons. Even 4 K blackbody photons have enough energy to break a Cooper pair. Adequate shielding is possible on the time scale of our computer. Inductive coupling to bodies of normal metal has to be avoided. By decoupling the qubit from electrical potentials, we have eliminated coupling to charged defects in substrate or tunnel barriers. The aluminum nuclei have a spin that is not polarized by the small magnetic fields at our temperature of 25 mK. Statistical fluctuations will occur, but their time constant is very long because of the absence of electronic quasi-particles. The net effect will be a small static offset of the level splitting, within the scale of the variations due to fabrication. The dephasing time that results from unintended dipole-dipole coupling of qubits is longer than 1 ms if the qubits are farther apart than 1 μm . Emission of photons is negligible for the small loop. Overall, the sources of decoherence that we know allow for a decoherence time above 1 ms.

Requirements for a quantum computer are that the qubits can be prepared in well-defined states before the start of the computation and that their states can be measured at the end. Initialization will proceed by cooling the computer to below 50 mK and having the qubits settle in the ground state. For the measurement, a generated flux of $10^{-3}\Phi_0$ in an individual qubit can be detected with a SQUID if enough measuring time is available. A good SQUID has a sensitivity of $10^{-5}\Phi_0/\text{Hz}^{1/2}$, so that a time of 100 μs is required. Usual SQUIDS have junctions that are shunted with normal metal. The shunt introduces severe decoherence in a qubit when the SQUID is in place, even if no measurement is performed. We are developing a nonshunted SQUID that detects its critical current by discontinuous switching. For a measurement at the end of a quantum computation scheme, the qubit can be frozen by an adiabatic increase of the tunnel barrier between the two qubit states. As Fig. 2 indicates, we can increase the barrier by a change of control current. A similar procedure, as suggested by Shnirman and Schön (14), for charge qubits can be followed.

The proposed qubit should be of considerable interest for fundamental studies of macroscopic quantum coherence, apart from its quantum computing potential. Compared with the radio frequency SQUID systems that have been used in attempts to observe such effects (16) and also have been suggested as possible qubits for quantum computation (17), the much smaller size of the qubit decouples it substantially better from the environment.

References and Notes

1. S. Lloyd, *Science* **261**, 1569 (1993).
2. C. H. Bennett, *Phys. Today* **48** (no. 10), 24 (1995); D. P. DiVincenzo, *Science* **270**, 255 (1995); T. P. Spiller, *Proc. IEEE* **84**, 1719 (1996).
3. S. Lloyd, *Sci. Am.* **273** (no. 4), 140 (1995).
4. Q. A. Turchette, C. J. Hood, W. Lange, H. Mabuchi, H. J. Kimble, *Phys. Rev. Lett.* **75**, 4710 (1995).
5. C. Monroe, D. M. Meekhof, B. E. King, W. M. Itano, D. J. Wineland, *ibid.*, p. 4714.
6. N. A. Gershenfeld and I. L. Chuang, *Science* **275**, 350 (1997).
7. B. Kane, *Nature* **393**, 133 (1998).
8. D. Loss and D. DiVincenzo, *Phys. Rev. A* **57**, 120 (1998).
9. L. B. Ioffe, V. B. Geshkenbein, M. V. Feigel'man, A. L. Fauchère, G. Blatter, *Nature* **398**, 679 (1999).
10. D. V. Averin and K. K. Likharev, in *Mesoscopic Phenomena in Solids*, B. L. Altshuler, P. A. Lee, R. A. Webb, Eds. (North Holland, Amsterdam, 1991), pp. 173–271.
11. W. J. Elion, M. Matters, U. Geigenmuller, J. E. Mooij, *Nature* **371**, 594 (1994); L. S. Kuzmin and D. B. Haviland, *Phys. Rev. Lett.* **67**, 2890 (1991); P. Joyez, D. Esteve, M. H. Devoret, *ibid.* **80**, 1956 (1998).
12. Y. Nakamura, Yu. A. Pashkin, J. S. Tsai, *Nature* **398**, 786 (1999).
13. A. Shnirman, G. Schön, Z. Hermon, *Phys. Rev. Lett.* **79**, 2371 (1997); D. V. Averin, *Solid State Commun.* **105**, 659 (1998); Yu. Makhlin, G. Schön, A. Shnirman, *Nature* **398**, 305 (1999).
14. A. Shnirman and G. Schön, *Phys. Rev. B* **57**, 15400 (1998).
15. T. P. Orlando *et al.*, in preparation.
16. C. D. Tesche, *Phys. Rev. Lett.* **64**, 2358 (1990); R. Rouse, S. Han, J. E. Lukens, *ibid.* **75**, 1614 (1995).
17. M. F. Bocko, A. M. Herr, M. J. Feldman, *IEEE Trans. Appl. Supercond.* **7**, 3638 (1997).
18. We thank J. J. Mazo, C. J. P. M. Harmans, A. C. Wallast, and H. Tanaka for important discussions. This work is partially supported by Army Research Office grant DAAG55-98-1-0369, Stichting voor Fundamenteel Onderzoek der Materie, NSF Award 67436000IRG, and the New Energy and Industrial Technology Development Organization.

22 April 1999; accepted 7 July 1999

Energetic Iron(VI) Chemistry: The Super-Iron Battery

Stuart Licht,* Baohui Wang, Susanta Ghosh

Higher capacity batteries based on an unusual stabilized iron(VI) chemistry are presented. The storage capacities of alkaline and metal hydride batteries are largely cathode limited, and both use a potassium hydroxide electrolyte. The new batteries are compatible with the alkaline and metal hydride battery anodes but have higher cathode capacity and are based on available, benign materials. Iron(VI/III) cathodes can use low-solubility K_2FeO_4 and BaFeO_4 salts with respective capacities of 406 and 313 milliampere-hours per gram. Super-iron batteries have a 50 percent energy advantage compared to conventional alkaline batteries. A cell with an iron(VI) cathode and a metal hydride anode is significantly (75 percent) rechargeable.

Improved batteries are needed for various applications such as consumer electronics, communications devices, medical implants, and transportation needs. The search for higher capacity electrochemical storage has focused on a wide range of materials, such as carbonaceous materials (1), tin oxide (2), grouped electrocatalysts (3), or macroporous minerals (4). Of growing importance are rechargeable (secondary) batteries such as metal hydride (MH) batteries (5), which this year have increased the commercial electric car range to 250 km per charge. In consumer electronics, primary, rather than secondary, batteries dominate. Capacity, power, cost, and safety factors have led to the annual global use of approximately 6×10^{10} alkaline or dry batteries, which use electrochemical storage based on a Zn anode, an aqueous electrolyte, and a MnO_2 cathode, and which

constitute the vast majority of consumer batteries. Despite the need for safe, inexpensive, higher capacity electrical storage, the aqueous MnO_2/Zn battery has been a dominant primary battery chemistry for over a century. Contemporary alkaline and MH batteries have two common features: Their storage capacity is largely cathode limited and both use a KOH electrolyte.

We report a new class of batteries, referred to as super-iron batteries, which contain a cathode that uses a common material (Fe) but in an unusual (greater than 3) valence state. Although they contain the same Zn anode and electrolyte as conventional alkaline batteries, the super-iron batteries provide >50% more energy capacity. In addition, the Fe(VI) chemistry is rechargeable, is based on abundant starting materials, has a relatively environmentally benign discharge product, and appears to be compatible with the anode of either the primary alkaline or secondary MH batteries.

The fundamentals of MnO_2 chemistry continue to be of widespread interest (6). The storage capacity of the aqueous MnO_2/Zn

Department of Chemistry and Institute of Catalysis Science, Technion—Israel Institute of Technology, Haifa 32000, Israel.

*To whom correspondence should be addressed. E-mail: chrlicht@technix.technion.ac.il

battery is limited by the charge capacity of MnO_2 [308 milliampere hours per gram ($\text{mA}\cdot\text{hours/g}$)], compared to that of Zn (820 $\text{mA}\cdot\text{hours/g}$). Alternative cathodes, such as Ag or air, have found only limited application because of their cost and power density limitations, respectively. Unusual cathodes, such as aqueous S (7), can inhibit the discharge behavior of conventional anodes such as oxidation of Zn to zincates. The aqueous MnO_2/Zn battery continues to contain either an ammonium chloride electrolyte (developed around 1860), an acidic chloride electrolyte, or, more recently, an alkaline electrolyte. In the latter, the electrolyte is not consumed during discharge, which increases the energy storage capacity. Additionally, the high alkaline conductivity can improve battery performance in the high-power domain (8). An attractive replacement will have higher capacity than MnO_2 , but will remain compatible with the Zn anode and the alkaline electrolyte. Alternative cathodes that we studied use Fe(VI) compounds. Because of their highly oxidized Fe basis, multiple electron transfer, and high intrinsic energy, we refer to the new cell containing these compounds as a “super-iron” battery.

Iron typically occurs as a metal, or in the valence states Fe(II) or Fe(III). Although the Fe(VI) species has been known for more than a century, its chemistry remains relatively unexplored (9), evidently due to a misperception that the Fe(VI) species is intrinsically highly unstable. The decomposition of Fe(VI) occurs in reactions such as those presented in Eq. 1. Indeed, the rapid decomposition of Fe(VI) to the environmentally benign ferric

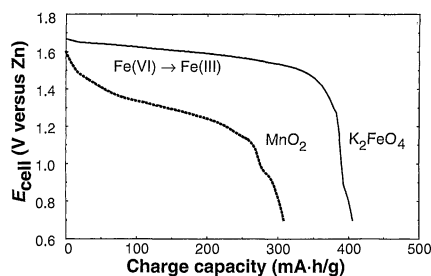
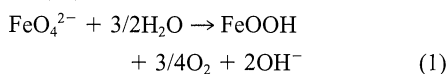
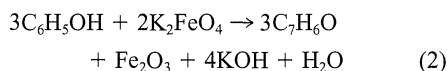


Fig. 1. Galvanostatic discharge at 0.5 mA/cm^2 of a K_2FeO_4 cathode compared to a MnO_2 cathode-limited Zn cell. Cell discharge was measured with Labview Software–interfaced Pine model AFCBP1 bipotentiostat at 22°C . The cathode consisted of either 17.3 mg ($7 \text{ mA}\cdot\text{hours}$) K_2FeO_4 or 22.7 mg ($7 \text{ mA}\cdot\text{hours}$) MnO_2 , mixed with 30% graphite by weight. In each case, a commercial 1.1-cm -diameter button cell containing excess Zn was opened, and the cathode was removed and replaced with the $7\text{-mA}\cdot\text{hours}$ cathode. Under these conditions, but at a higher current density of 5 mA/cm^2 , the faradaic efficiency of a K_2FeO_4 cathode, discharged to 1 V , falls to 66% of the theoretical capacity of $406 \text{ mA}\cdot\text{hours/g}$, whereas a BaFeO_4 cathode generates 85% of its theoretical capacity ($313 \text{ mA}\cdot\text{hours/g}$).

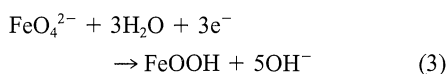
oxide product via Eq. 1 has been the basis for suggesting the use of Fe(VI) as a safer alternative to the chlorination purification of water (10)



Similarly, the strong oxidizing nature of Fe(VI) has been suggested for the oxidative preparation of a variety of organic compounds (11), including conditions for the oxidation of benzyl alcohol to benzaldehyde at 100% yield (12)

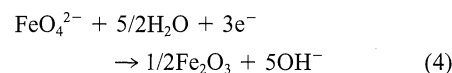
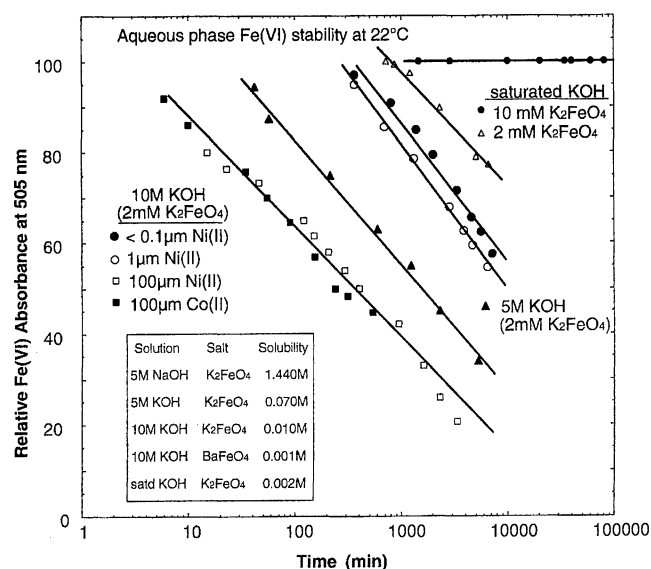


The reduction of Fe(VI) represents an energetic and high-capacity source of cathodic charge. We have investigated a variety of salts, including those with the following theoretical three-electron charge capacities determined as $3F \times \text{MW}^{-1}$, from the salt molecular weight, $\text{MW}(\text{g/mol})$ and the Faraday constant ($F = 96,485 \text{ coulomb/mol} = 26,801 \text{ mA}\cdot\text{hours/mol}$): K_2FeO_4 ($406 \text{ mA}\cdot\text{hours/g}$), Na_2FeO_4 ($485 \text{ mA}\cdot\text{hours/g}$), Li_2FeO_4 ($601 \text{ mA}\cdot\text{hours/g}$), Cs_2FeO_4 ($209 \text{ mA}\cdot\text{hours/g}$), SrFeO_4 ($388 \text{ mA}\cdot\text{hours/g}$), Ag_2FeO_4 ($240 \text{ mA}\cdot\text{hours/g}$), MgFeO_4 ($558 \text{ mA}\cdot\text{hours/g}$), CaFeO_4 ($503 \text{ mA}\cdot\text{hours/g}$), BaFeO_4 ($313 \text{ mA}\cdot\text{hours/g}$), and ZnFeO_4 ($434 \text{ mA}\cdot\text{hours/g}$). The discharge of these solid materials as battery cathodes has not been previously reported. In particular, pure K_2FeO_4 and BaFeO_4 are readily synthesized (13). The K_2FeO_4 cathodic charge capacity is 32% greater than the equivalent MnO_2 . The full $406 \text{ mA}\cdot\text{hours/g}$ storage capacity of K_2FeO_4 is obtained during discharge (Fig. 1), in accord with



or as the anhydrous product

Fig. 2. Stability of Fe(VI) (1 week = 10,800 min), as measured by variation of the aqueous FeO_4^{2-} absorption occurring at 505 nm , and our measured 505-nm extinction coefficient $\epsilon_{505\text{nm}}(\text{FeO}_4^{2-})$ of $1.1 \text{ mM}^{-1} \text{ cm}^{-1}$. A relative absorption of 100 (as a percentage) refers to the initial FeO_4^{2-} concentration. Colloidal ferric oxide is generated if Fe(VI) decomposes. This interference is minimized by a 385-nm baseline correction and solution centrifugation before spectroscopic analysis. The indicated Ni(II) and Co(II) concentrations are prepared as added nitrate salts.



The BaFeO_4 , although of lower capacity than K_2FeO_4 , discharges a higher fraction of this charge at higher current densities (Fig. 1 legend). Both Fe(VI) materials were used as synthesized. As exemplified by the history of MnO_2 optimization, Fe(VI) coulombic efficiency will be further affected by additives other than graphite, and control of packing, electrolyte, and particle size (14). The average discharge potential of the K_2FeO_4 cathode of 1.58 V versus Zn is 24% greater than the average for the equivalent MnO_2 cell (1.27 V), both determined to 90% depth of discharge (Fig. 1). Combined with the increased charge capacity, this potential also leads to a further increase in comparative energy capacity.

The fundamental solubility and stability constraints on FeO_4^{2-} chemistry are not well established. The BaFeO_4 and K_2FeO_4 Fe(VI) salts both combine attributes of very low alkaline solubility (Fig. 2, data inset) and high stability. Alternatively, Li_2FeO_4 and Na_2FeO_4 exhibit high solubilities ($\sim 1 \text{ M}$) in alkaline hydroxide. The synthesized K_2FeO_4 is stable in a dehumidified environment and is readily mixed with graphite and molded as a cathode under pressure. The synthesized BaFeO_4 is highly stable in a humid environment and may be either pressed or formed as a paste.

The view of Fe(VI) species as intrinsically unstable is not correct. For example, an excess of K_2FeO_4 in contact with a concentrated KOH solution has a calculated stability of many years. Veprek-Siska and Ettl demonstrated that at elevated temperatures, the rapid decomposition of Fe(VI) is due to trace catalysis by Ni(II) and concluded “the rate of non-catalyzed decomposition is immeasur-

REPORTS

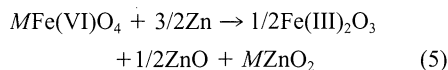
ably low" (15). We studied stability at room temperature (Fig. 2), by measuring the 505-nm wavelength peak absorption of FeO_4^{2-} . In 10 M KOH, the stability of K_2FeO_4 is increased by orders of magnitude, from hours to weeks, when the concentration of Ni(II) is decreased from 100 μM to $<0.1 \mu\text{M}$. The K_2FeO_4 exhibits similar stability in KOH or NaOH (16) electrolytes. We observed that the catalyzed kinetics are first order for FeO_4^{2-} concentration. Hence, the half life of 0.001 M is the same as for 0.01 M K_2FeO_4 , in solutions containing constant Ni(II) and OH^- concentrations.

The catalytic acceleration of Fe(VI) decomposition in solution is evident with $<1 \mu\text{M}$ Ni(II). At the lowest Ni(II) concentrations, solution pretreatment (such as inducing decomposition of 2 mM K_2FeO_4 in KOH solution at 60° to 80°C , followed by removal of the decomposition products) can improve the subsequent Fe(VI) stability. Nickel(II) and Co(II) exhibit similar catalytic effects (Fig. 2). However, we observed no other significant catalytic activity for salts not containing Ni(II) or Co(II), including the nitrates of added Cu(II), Fe(III), Zn(II), Pb(II), Ba(II), Sr(II), Ca(II), Mg(II), or other salts including $\text{K}_2\text{Zn}(\text{OH})_4$, KIO_4 , $\text{K}_2\text{B}_4\text{O}_7$, K_3PO_4 , $\text{Na}_4\text{P}_2\text{O}_7$, Na_2SiF_6 , Na_2SiO_3 , Na_2MoO_4 , or Na_2WO_4 .

The observed stability of Fe(VI), as FeO_4^{2-} , is an order of magnitude greater in 10 M KOH compared to 5 M KOH. Continuing this trend, Fe(VI) is further stabilized in saturated ($\sim 13.5 \text{ M}$) KOH (Fig. 2). We correlate this phenomenon to a decrease in Ni(II) and Co(II) activity with an increase in hydroxide activity, as determined from the solubility product $K_{\text{sp}}[\text{Ni}(\text{OH})_2] \approx K_{\text{sp}}[\text{Co}(\text{OH})_2] \approx 10^{-15}$ and the tendency toward formation of these metal ions as the tri- and tetra-hydroxymetallates in concentrated hydroxide solutions. In this saturated KOH solution, Fe(VI) decomposes at a rate of 10^{-9} M/s . This rate is equivalent, in 1 ml of this solution, to a monthly loss of 0.0005 g K_2FeO_4 . Hence in this solution, excess 10 mM (solubility 2 mM) K_2FeO_4 , exhibits no change in absorbance at 505 nm for the measured period of 3 months (Fig. 2). This solution is prepared with 0.002 g/ml K_2FeO_4 . However, a battery contains a much larger fraction of cathode mass, typically $>1 \text{ g}$ cathode per milliliter electrolyte. Extension of the data collected over a few months to predict behavior in 10 years is risky, but based on the measured solution-phase Fe(VI) decomposition rate, after 10 years there will be less than a 10% loss of 1 g K_2FeO_4 in contact with 1 ml concentrated KOH solution.

In a Zn alkaline battery the Zn anode generates a distribution of zinc oxide and zincate products, and similarly, the final Fe(VI) product will depend on the depth of discharge. For the respective K and Ba super-

iron batteries, the cell discharge reaction may be generalized with $M = \text{K}_2$ or Ba as



Equation 5 shows that OH^- generated during reductive discharge closely balances that consumed by a Zn anode. This is compatible with our observation that little electrolyte is required in the complete Fe(VI) storage cell.

A variety of super-iron Zn batteries have been prepared and discharged. The open-circuit potential observed in the super-iron Zn battery is modified by $\pm 0.05 \text{ V}$ with variation of packing conditions and electrolyte. Generally, the BaFeO_4 potential, at 1.85 V, is 0.1 V higher than the K_2FeO_4 battery at 1.75 V. On the basis of these open-circuit potentials and Eq. 5, the $\text{K}_2\text{FeO}_4/\text{Zn}$ and BaFeO_4/Zn batteries have a

respective maximum energy capacity of 475 W-hours/kg, and 419 W-hours/kg, both higher than the maximum of 323 W-hours/kg for a MnO_2/Zn battery; other Fe(VI) compounds suggest further storage capacity increases.

The energy capacities of several Fe(VI) and conventional MnO_2 cathode, alkaline primary batteries with a Zn anode have been measured and compared (Fig. 3). In both the low- (6000 ohm, current density $J \approx 0.25 \text{ mA/cm}^2$) and high- (500 ohm, $J \approx 3 \text{ mA/cm}^2$) discharge domain, the K_2FeO_4 cell generates significantly higher capacity than does the MnO_2 cell. Of the three cells examined, the BaFeO_4 cathode cell exhibits the highest coulombic efficiency at high discharge rates ($J > 10 \text{ mA/cm}^2$), resulting in the observed higher energy capacity despite the lower intrinsic charge capacity of BaFeO_4 compared to K_2FeO_4 .

Fig. 3. Energy capacity of several super-iron and conventional MnO_2 cathode alkaline primary batteries with a Zn anode. In each case, a constant discharge load is used of either 150, 500, or 6000 ohms. The MnO_2 cells consist of conventional (commercial) 1.1-cm-diameter alkaline button cells rated at 31 mA-hours capacity. Super-iron cells were prepared by opening alkaline button cells and replacing the cathode with 31 mA-hours of either (i) 90% (76.3 mg) K_2FeO_4 , 10% (9 mg) graphite, and 12 mg concentrated KOH, or (ii) 90% (106 mg) BaFeO_4 , 10% (12 mg) graphite, and 30 mg concentrated KOH. Energy capacity is calculated from the mass of the anode, wet separator, and total cathode mass.

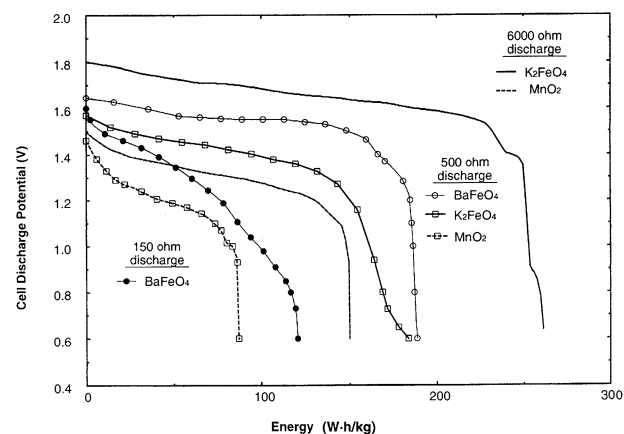
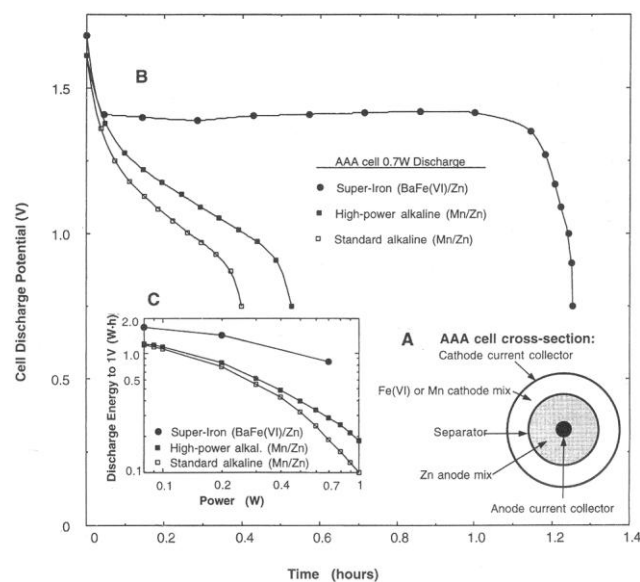


Fig. 4. The discharge of super-iron (BaFeO_4) compared to the discharge of standard or high-power alkaline MnO_2 , each in AAA (cylindrical) cell configuration. (A) Cell cross-section. Total diameter is 10.1 mm, and height (76) of the cathode current collector is 42 mm. In the super-iron AAA experiments, components were removed from the standard alkaline cell, and the outer MnO_2 mix was replaced with a pressed BaFeO_4 mix (containing 90% BaFeO_4 , 10% conductor, and 0.4 ml saturated KOH). This was followed by inclusion of the separator, Zn anode mix, and anode collector. (B) The cell potential measured during constant power discharge. (C) Measured energy capacity (watt-hour) versus power (watt) for the super-iron, high-power, or standard alkaline MnO_2 AAA cells. The data for the latter two cells is from (17).



The benefit of the facile charge-transfer capabilities of the conductive BaFeO_4 salt is evident in a cylindrical cell configuration (Fig. 4). Discharged to 1 V at 0.7 W high constant power, the BaFeO_4 cell provides 200% higher energy compared to advanced MnO_2 alkaline cylindrical AAA cells (0.86 W-hours compared to 0.285 W-hours). Common cylindrical cells range in volume from approximately 3 to 50 cm^3 for AAA up to D-type configurations. This geometry requires an increase in material scale by two orders of magnitude compared to the simple "button" configuration, and provides an ongoing challenge in cell optimization. Industry regularly reports incremental increases in alkaline cylindrical MnO_2/Zn energy density and, most recently, has reported advances in the high-power discharge domain. One recent post-ed advanced result is determined at constant power discharge (Fig. 4, inset) (17). Compared to these conventional advanced alkaline cells, the BaFeO_4 cell provides a 200% higher energy capacity under high-drain (0.7 W discharge) and a 40% increased capacity under low-drain (0.08 W) conditions. The cylindrical BaFeO_4 cell uses the conventional cell Zn anode mix, anode current collector, and separator. In future experiments; with specific optimization for the super-iron cell, further energy capacity increases are expected.

Conventional MH batteries, with a capacity up to 95 W-hours/kg (5), compared to 40 W-hours/kg for NiCd, have advanced to where further energy storage improvements are largely limited by the cell's heavy nickel oxyhydroxide (NiOOH) cathode. This situation is analogous to the limitations of MnO_2 for primary Zn batteries and is accentuated by the lower limiting NiOOH cathode capacity of ~ 290 mA-hours/g. These important secondary (rechargeable) batteries use alkaline KOH electrolyte.

We have also probed the reversible nature of Fe(VI) chemistry. An Fe(VI) charge-limited open-cell experiment provides fundamental evidence that the Fe(VI) cathode is significantly rechargeable. The cell has been discharged to 75% cathode capacity depth of discharge (DOD) for several cycles and more than 400 cycles at 30% DOD. The cell consists of an excess of MH anode (35 mA-hours, removed from a GP 35BVH button cell), and a limiting Fe(VI) cathode (9 mA-hours based on 406 mA-hours/g K_2FeO_4 , using a Teflon mesh pressed over the K_2FeO_4 mix), in excess 12 M KOH electrolyte. The cell potential varies from 1.3 V (open circuit) to 1.1 V (at 5 mA/cm²) and is cycled at 2.5 mA charge and 1 mA discharge. This cell has a characteristic voltage similar to the conventional MH battery because of the similarity of the Fe(VI) potential to the 0.5 V formal potential of NiOOH .

In the primary-battery studies, the AAA cell configuration has been used only to pro-

vide a clear comparison to existing optimized electrochemistries. The engineering of MnO_2 into a conventional cylindrical cell is an ongoing process which has taken many decades. Engineering studies of the new Fe(VI) cathode will also be an ongoing process. Further research probing, stabilizing, and releasing the substantial storage of other Fe(VI) cathodes will be needed. For example, a composite high-capacity Fe(VI) cathode containing several Fe(VI) salts also exhibits efficient discharge in the high-current domain, and, as in the K_2FeO_4 and BaFeO_4 cells in this study, generates significantly greater energy capacity than in conventional alkaline batteries.

References and Notes

1. J. R. Dahn, T. Zheng, Y. Liu, J. S. Xue, *Science* **270**, 590 (1995).
2. Y. Idota, T. Kubota, A. Matsufoji, Y. Maekawa, T. Miyasaka, *ibid.* **276**, 1395 (1997).
3. E. Reddington *et al.*, *ibid.* **280**, 1735 (1998).
4. B. T. Holland, C. F. Blanford, A. Stein, *ibid.* **281**, 538 (1998).
5. S. R. Ovshinsky, M. A. Fetchenko, J. Ross, *ibid.* **260**, 176 (1993); S. K. Dhar *et al.*, *J. Power Sources* **65**, 1 (1997).
6. Z. Rong *et al.*, *Science* **276**, 926 (1997).
7. D. Peramunage and S. Licht, *ibid.* **261**, 1029 (1993).
8. S. Licht, D. Peramunage, N. Myung, *J. Phys. Chem. B* **102**, 6780 (1998).
9. M. D. Johnson and J. F. Read, *Inorg. Chem.* **35**, 6795 (1996).
10. J. D. Carr *et al.*, Proceedings of the 5th Conference, *Water Chlorination*, Williamsburg, VA, 3 to 8 June

1984, R. L. Jolley, Ed., (Lewis, Chelsea, MI, 1985), pp. 1285–1298; V. K. Sharma, J. O. Smith, F. J. Millero, *Environ. Sci. Technol.* **31**, 2486 (1997).

11. M. D. Johnson and B. Hornstein, *Chem. Commun.* **1996**, 965 (1996).
12. L. Delaude and P. A. Laszlo, *J. Org. Chem.* **61**, 6360 (1996).
13. Using analytical grade reagents of 97 to 99% purity, K_2FeO_4 was synthesized from alkaline hypochlorite treatment of $\text{Fe}(\text{NO}_3)_3$ as described in (12). The dried product is stable in time. The BaFeO_4 was synthesized from 0.25 M (97 to 99% pure) K_2FeO_4 dissolved in 2% KOH solution at 0°C, and filtered into an equivalent volume of 0.39 M (analytical grade) $\text{Ba}(\text{C}_2\text{H}_3\text{O}_2)_2$ solution at 0°C. Solutions were prepared without CO_2 in deionized water. The precipitate was filtered, washed with water, and freeze dried (using a Labconco Lyph-Lock Freeze Dry System), producing 98.5 \pm 0.5% purity BaFeO_4 . The Li_2FeO_4 , Na_2FeO_4 , and Cs_2FeO_4 were prepared in a manner similar to K_2FeO_4 (hypochlorite oxidation) but yielded lower purity. The SrFeO_4 , Ag_2FeO_4 , MgFeO_4 , CaFeO_4 , and ZnFeO_4 were investigated in a manner similar to BaFeO_4 (precipitation from a K_2FeO_4 solution) but yielded lower purity.
14. J. Chen and H. Y. Che, *J. Electrochem. Soc.* **140**, 1205 (1993).
15. J. Veprek-Siska and V. Ettl, *Chem. Ind.* **1967**, 548 (1967).
16. S. Licht, B. Wang, S. Ghosh, data not shown.
17. Duracell Web site, file MX2400.pdf (ULTRA vs. Standard AAA) downloaded 24 June 1999. (www.duracell.com/OEM/Primary/Alkaline/alkaline_manganese_data.html).
18. We thank V. Naschitz, J. Li, S. Shesternin, and V. Nair, who participated in synthesis of the Fe(VI) compounds, and G. Xu, V. Goldstein, O. Khaselev, and E. Kvashnina who participated in cell discharges.

25 May 1999; accepted 2 July 1999

Phonon- Versus Electron-Mediated Desorption and Oxidation of CO on Ru(0001)

M. Bonn,* S. Funk, Ch. Hess, D. N. Denzler, C. Stampfl, M. Scheffler, M. Wolf, G. Ertl

Heating of a ruthenium surface on which carbon monoxide and atomic oxygen are coadsorbed leads exclusively to desorption of carbon monoxide. In contrast, excitation with femtosecond infrared laser pulses enables also the formation of carbon dioxide. The desorption is caused by coupling of the adsorbate to the phonon bath of the ruthenium substrate, whereas the oxidation reaction is initiated by hot substrate electrons, as evidenced by the observed subpicosecond reaction dynamics and density functional calculations. The presence of this laser-induced reaction pathway allows elucidation of the microscopic mechanism and the dynamics of the carbon monoxide oxidation reaction.

The catalytic oxidation of CO on transition metal surfaces is technologically very important, being a key reaction, for example, in automotive exhaust catalysts. To fully under-

stand this surface reaction—ideally leading to better and more efficient catalytic processes—requires insight on atomic length (angstrom) and reaction time (femtosecond) scales. Structural information with the required spatial resolution has recently been obtained by means of scanning probe techniques (1), but the ultrafast dynamics (2) of such reactions are still largely unexplored,

Fritz-Haber-Institut der Max-Planck-Gesellschaft, Faradayweg 4-6, 14195 Berlin, Germany.

*To whom correspondence should be addressed. E-mail: bonn@fhi-berlin.mpg.de